

Optical Engineering

OpticalEngineering.SPIEDigitalLibrary.org

Micromechanical analysis of inclusions in particulate media using digital photo stress analysis tomography

Simon Joseph Antony
Osas Imafidon
Thabit Barakat

Micromechanical analysis of inclusions in particulate media using digital photo stress analysis tomography

Simon Joseph Antony,^{a,*} Osas Imafidon,^a and Thabit Barakat^b

^aUniversity of Leeds, Institute of Particle Science and Engineering, School of Chemical and Process Engineering, Leeds, LS2 9JT, United Kingdom

^bKing Saud University, College of Science, Department of Physics and Astronomy, PO Box 2455, Riyadh, Saudi Arabia

Abstract. An experimental study aimed at sensing the stress distribution characteristics of inclusions inside particulate assemblies subjected to axial compaction is presented. The particulate assemblies are made of powders and grains, in which photoelastic inclusions are embedded along the central axis of the assemblies at different elevations. Digital photo stress analysis tomography is used to obtain the contours of maximum shear-stress distribution and the direction of major principal stress within the inclusions under the external loading. Using this, an analysis is performed for understanding the implications of using Hertz theory based on discrete element modeling for simulating stresses in relatively big inclusions surrounded by particulates. In the case of the inclusions surrounded by the grains, the location at which the peak value in maximum shear stresses occurs within the inclusions deviates from that of Hertzian analysis. This effect is dominant in the case of inclusions residing close to the loading surface. Unlike granular materials, shear-stress distribution characteristics of inclusions in powder surroundings tend to display continuum-like behavior under external compression and points to the need for a deeper understanding of the effects of the surrounding materials in particulate beds with inclusions. © 2015 Society of Photo-Optical Instrumentation Engineers (SPIE) [DOI: [10.1117/1.OE.54.8.081202](https://doi.org/10.1117/1.OE.54.8.081202)]

Keywords: micromechanics; digital photoelasticity; photo stress analysis tomography; discrete element modeling; powders; granular materials.

Paper 141200SS received Jul. 25, 2014; revised manuscript received Aug. 29, 2014; accepted for publication Sep. 2, 2014; published online Feb. 26, 2015.

1 Introduction

Micromechanical analysis of particulate materials, such as powders and grains, has been of significant interest to academic and industrial communities, from beach sandcastles to chemical, pharmaceutical, food, geotechnical, mechanical, minerals, and materials processing sectors. Particulate media are composed of discrete particles, usually with different particle-scale properties and interparticle interactions, that are responsible for their complex behaviors at the macroscopic scale.^{1,2} Under different external loading environments, particulate media exhibit a variety of unusual characteristics at both microscopic and macroscopic scales which make them different from conventional solids, liquid, and gaseous matter.³ Advanced particulate modeling methods, such as discrete element modeling (DEM) and molecular dynamics, have helped in understanding the microscopic origin of shear strength in particulate assemblies.³ In particulate assemblies, force transmission occurs via interparticle contacts in a non-homogeneous manner even under a homogeneous external loading environment. Under loading, particulate materials mobilize shear strength due to the contributions of only a small proportion (c.a. 25%) of all available contacts; these are referred to as strong contacts.^{4,5} The remaining contacts (weak contacts) contribute to support the strong force-transmitting contacts. Studies based on photoelastic experiments⁶⁻⁸ have also reported nonhomogeneous distribution of stress-transmitting contacts³ in granular assemblies under external loading environments. Such observations are supported by computational methods such as DEM, in which

the micro-macro relationships of stresses are developed by averaging techniques⁹ over the required subgroup of interparticle contacts¹⁰ based on a statistical mechanics principle. In such calculations, multiple-interaction effects of contacts are usually not rigorously accounted. For example, using DEM it is difficult to obtain information on the nature of stress distribution “within” the particles. In DEM, stress calculations are performed using the interparticle contact forces while ignoring the distribution of them within the single-particle scale. To perform this task, one would have to couple DEM with other computational methods such as finite-element modeling (FEM), which is computationally intensive and often expensive. Further, DEM modeling of particulate systems with relative large inclusions in comparison with the size of surrounding particles is usually difficult to perform due to the computational difficulties associated with boxing⁹ (i.e., choosing the dimensions of the grids in such a way that the contributions of all surrounding particles are accounted for when computing the average stress tensor of the large inclusions).

Recently, an experimental study based on photo stress analysis tomography (PSAT) was used for understanding the influence of wall boundaries on the nature of shear stress experienced by an inclusion for the positions close to wall boundaries.¹¹ The study shows the effectiveness of using the inclusions as a sensor to identify the level of shear dominant zones close to the walls in particulate assemblies. Other experimental approaches have also been used to characterize particulate assemblies. These include x-ray micro tomography,¹² nuclear magnetic resonance imaging,¹³ and positron

*Address all correspondence to: Simon Joseph Antony, E-mail: S.J.Antony@leeds.ac.uk

emission particle tracking,¹⁴ but these are mostly aimed at probing the density and velocity distribution inside particulate samples. Visual information on how relatively big particulate inclusions sustain shear at different elevations inside a compaction chamber is still unclear. The current research addresses this challenge using digital PSAT methodology.

2 Background of Photo Stress Analysis Tomography

The working principles of photoelasticity methodology are well established.¹⁵ Induced stresses in birefringent materials cause a change in their refractive index. The application of photo stress analysis utilizes the induced birefringence of the material to examine the stress distribution within the objects under consideration. The direction and magnitude of the components of maximum shear stress at any point can be determined by utilizing the fringe patterns which characterize the retardation of light (between the principal optical axes) passing through the optical setup, i.e., a circular polariscope. Two different types of fringes can be observed: isochromatic and isoclinic fringes. Isochromatic fringes are lines of constant principal stress difference ($\sigma_{11} - \sigma_{33}$ where σ_{11} and σ_{33} are the major and minor principal stresses, respectively). The difference in the principal stresses at any point on the birefringent material, hence, the maximum shear stress, can be related to the fringe order using the stress-optics law.¹⁵ Isoclinic fringes occur whenever either principal stress direction coincides with the axis of polarization of the polarizer.¹⁵ Therefore, isoclinic fringes provide information about the directions of the principal stresses in the model. However, for convenience, they can be eliminated by using a circular polariscope¹⁵ (Fig. 1). Image capturing and digital image processing techniques¹⁶⁻¹⁹ allow for the separation of the isoclinic and isochromatic fringe patterns relatively more quickly. Hence, both the maximum shear stress and the directions of principal stresses can be obtained at any point of interest in the birefringent material. We wish to point out that, in particulate systems, even

linearly elastic grains could result in a nonlinear and plastic behavior at the bulk scale under mechanical loading. This could be due to the irreversible grain dislocations, which is an inherent property of discrete particulate systems. Hence, to avoid any confusion, an integrated (plane and circular) digital photoelastic tomography¹⁷⁻²⁰ is referred to as PSAT in particulate engineering.²¹

3 Experiments

Figure 2 shows the schematic diagram of the axial compression rig used in the experiments. A circular inclusion (Young modulus 2.9 GPa, Poisson's ratio 0.355 and stress fringe value 0.14 kN/mfringe) of diameter $d = 10$ mm and thickness 3.2 mm was positioned at different levels from the loading surface ($\lambda_v = 0, 1.75 d, 3.5$ and $7 d$), while the horizontal distance ($\lambda_h = 13 d$) remains constant from both ends of the wall. The wall and the loading pad (rigid) were made of a finely polished and smooth perspex sheet to minimize any frictional effects in this study. The depth of the particulate fillings inside the rig is $15 d$. The study is carried out for elastic inclusions (birefringent) embedded in two different cases of particulate packing with regard to the number of contacts surrounding the inclusion (coordination number):

- Type 1: Vigna Radiata granular packing [coordination number of sensor = 13, average particle size = 3 mm, packing density = 1170 kg/m^3 , angle of repose ~ 5 deg (noncohesive) (Fig. 2)]
- Type 2: Starch powder packing [Co-ordination number of the sensor $\sim \infty$, average particle size = $300 \mu\text{m}$, packing density = 650 kg/m^3 , angle of repose 45 deg (cohesive)]

Initially, particulate samples with the inclusion at the desired position were carefully prepared inside the compression rig as shown in Figs. 3 and 4 (size $270 \times 150 \times 3.2$ mm) using an identical filling procedure (carefully controlled layered type filling and random packing) such that the initial bulk density of the samples of a particular type of material

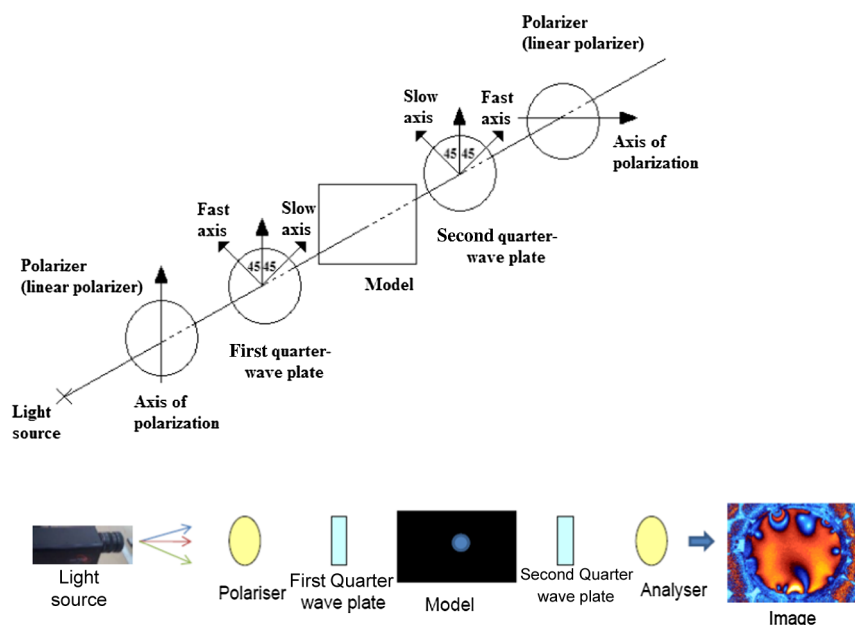


Fig. 1 Schematic diagram of a circular polariscope setup.

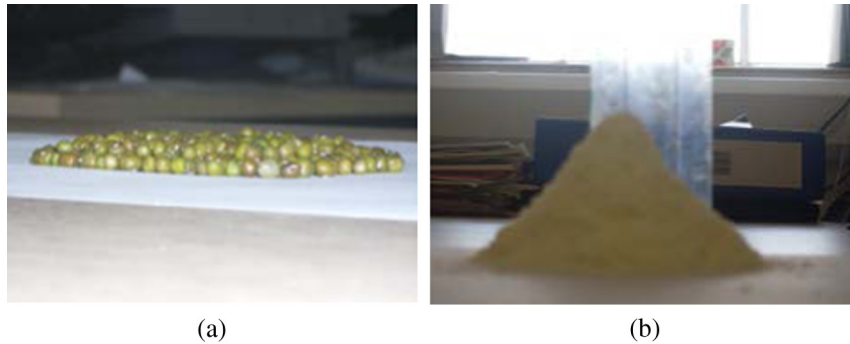


Fig. 2 (a) Grains and (b) powder materials used in determining the angle of repose.

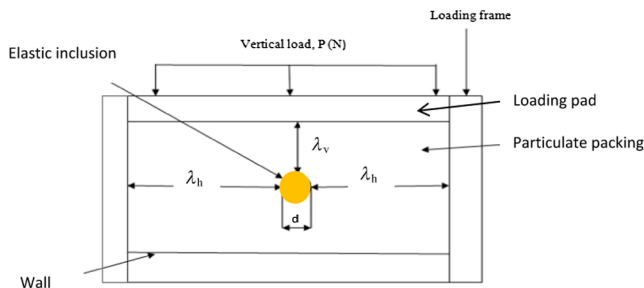


Fig. 3 Schematic diagram of the experimental loading rig.

was independent of the position of the inclusion. We initially verified the effects of filling the packing on the repeatability of the experimental observations made in this study. As the samples were consistently prepared, the experiments were repeatable and errors in the measurements were within about 5%. Axial loading (P) was applied in small increments (quasistatic compression) to the desired levels.

4 Analysis

The birefringent properties of the sensor particle were recorded and analyzed to obtain the distributions of maximum shear stress and direction of the principal stress for the experiments reported here.

4.1 Distribution of Maximum Shear Stresses within the Inclusions

The average distribution of maximum shear stress (τ_{max}) within the inclusion was determined by collecting birefringent data across four sections: 0 deg, 45 deg, 90 deg, and 135 deg

(Fig. 5). If a contact does not exist on these angular sections, the closest contact to them is considered. The starting point of the sections are always from the contacts identified as stated above and pass through the center of the disc to the point of their mirror image (finishing point). The results are presented in terms of the normalized depth of the inclusion, S where $S = r/d$.

4.2 Identifying the Location in the Inclusion Where Peak Value of Maximum Shear Stress Occurs

As mentioned above, the present study is also aimed at understanding some of the limitations in the current modeling techniques such as DEM using Hertz theory for defining interparticle contact interactions. This is performed by evaluating the distance at which maximum shear-stress peaks occur in the inclusion and this is compared to results using Hertz theory,²² which ignores any interaction effects of contiguous contacts (Fig. 5).

5 Results and Discussions

Figures 6 and 7 show the contours of maximum shear-stress distribution within the inclusions embedded in the granular and powder packing, respectively.

In these plots, the arrows indicate the direction of the major principle stress in the inclusions under different load levels and locations (λ_v) from the loading surface. The results show that an increase in the load levels results in an increase in the maximum shear stress in the inclusion embedded inside both cases of the packing. In the case of the inclusion residing inside the powder packing and close to the loading surface ($\lambda_v = 0$), even under the low load level it experienced a significant level of maximum

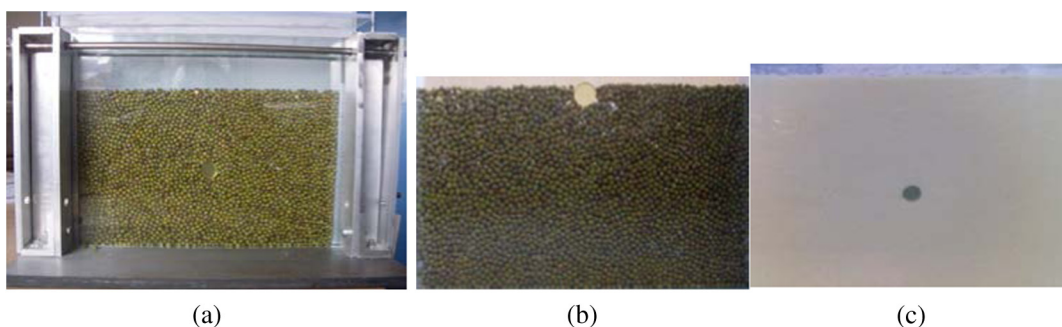


Fig. 4 Some examples showing the initial samples with the inclusion embedded inside the powder and granular beds. The inclusion is located at different positions (λ_v) from the top surface of the fillings: (a) $\lambda_v = 7$ cm (b) $\lambda_v = 0$ and (c) $\lambda_v = 7$ cm.

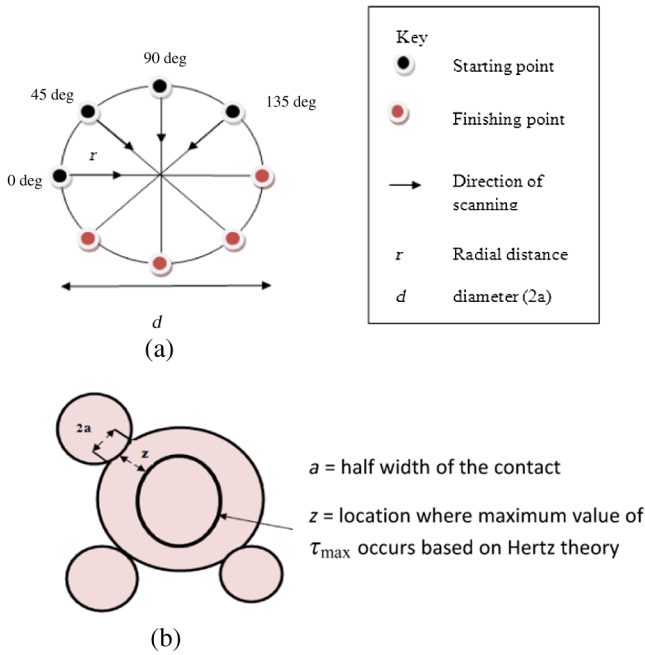


Fig. 5 Illustration showing (a) the directions of collecting data in the inclusion to determine average distribution of maximum shear stress and (b) location of maximum shear stress from a contact.

shear stress when compared with that of the granular packing. This suggests that the anisotropy in the stress transmitted through the contacts to the inclusion is relatively weaker in the case of granular surroundings than in the powder surroundings. This is also evident from the plots of the direction of the major principal stress in these inclusions. This trend is

also widely observed in the case of inclusions residing away from the loading surface. Hence, a powder surrounding generally tends to induce a stronger anisotropy than a granular surrounding in the inclusions under axial compression. Another interesting aspect is that the inclusions away from the loading surface in granular surroundings tend to show a much weaker maximum shear-stress distribution profile ($\lambda_v > 0$ in Fig. 6) when compared with that of powder surroundings (Fig. 7) under identical loading conditions. This suggests that the influence zone of shear in the powder bed spreads much deeper than in the case of the granular bed. However, far away from the loading surface ($\lambda_v = 7d$), the type of the surrounding does not have much influence on the maximum shear-stress distribution of the inclusion (Figs. 6 and 7), and hence displays a material independent behavior.

Now, we consider the tendency of the powder surroundings to induce a relatively more continuum-like behavior. For this, in Fig. 8 we present the maximum shear-stress distribution for two typical combinations of the loading and packing environments of the inclusions: (1) inclusions residing close to the loading surface under a low load level ($\lambda_v = 0$ and $P = 3.11$ N) and (2) inclusions residing away from the loading surface and under a relatively higher load level ($\lambda_v = 3.5d$ and $P = 7.52$ N). It is evident that in the case of the powder surrounding, the inclusion generally experiences a stronger anisotropy in bearing the shear stress. This is evident from the anisotropy in the direction of the major principal stress as shown in Figs. 8(a) and 8(b). This behavior is observed more dominantly in the case of an inclusion positioned away from the loading surface [Fig. 8(b)], in which the direction of the principal stress acts along the axial direction; it is much

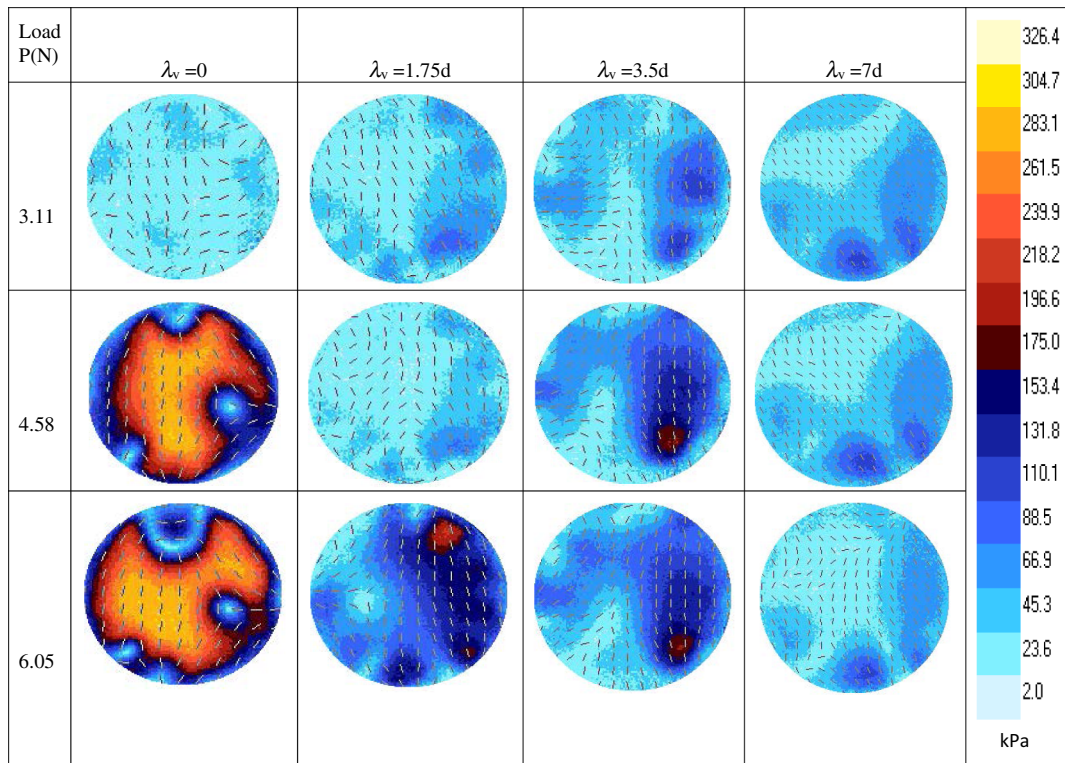


Fig. 6 Contours of maximum shear-stress distribution in the inclusion embedded in the granular assembly. The arrows show the direction of the major principal stress.

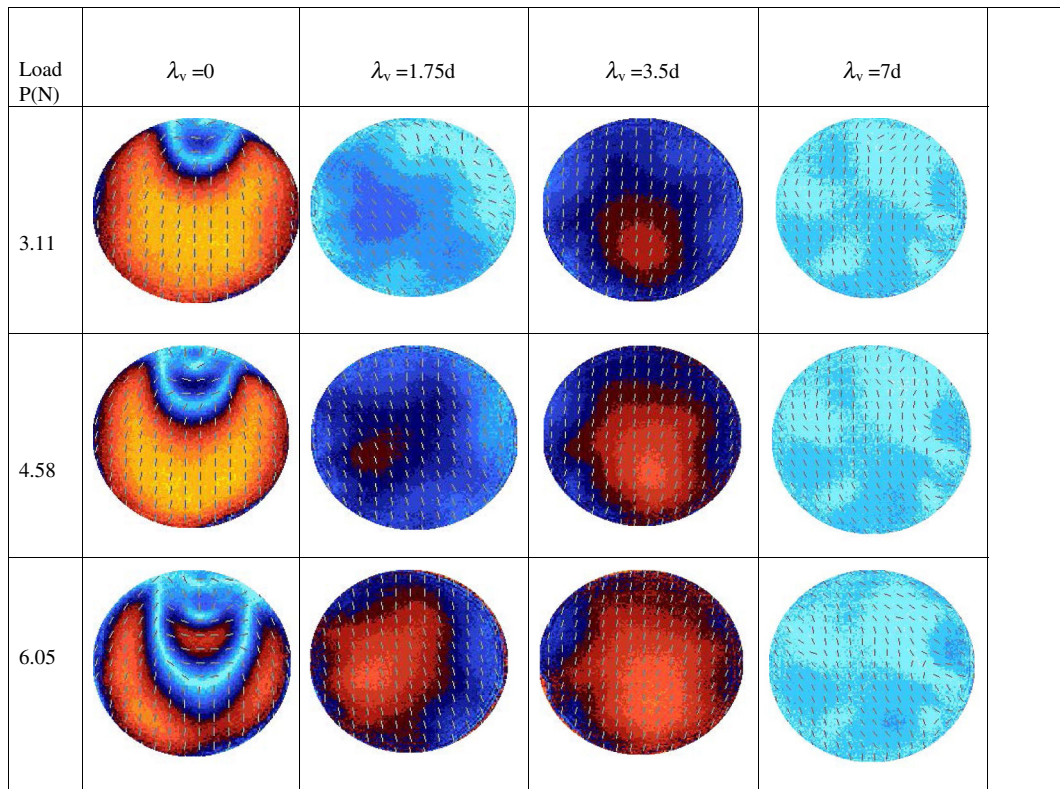


Fig. 7 Contours of maximum shear-stress distribution in the inclusion embedded in the powder assembly. The arrows show the direction of the major principal stress (color coded to the same scale as presented in Fig. 6).

more widely spread in relatively high magnitudes and displays a continuum-like behavior. The source point (from where shear contours originate and grow) is at the center of the inclusion, unlike in the case of granular packing where this occurs close to the boundary of the inclusion in a relatively less anisotropic manner. This would imply that the shear-dominant yielding and breakage of the inclusion are more likely to originate from the center of the inclusion inside the powder surrounding. The variation of maximum shear-stress distribution (average τ_{max}) in relation to the normalized depth (S) within the inclusion under different load levels, location (λ_v) and surrounding environments is presented in Fig. 9.

We observe the following: (1) in general, the distribution of maximum shear stress (τ_{max}) within the system is strongly nonhomogeneous within the inclusions for all load levels and locations in both particulate surroundings. It is strongly influenced by the closeness of the inclusion to the loading surface (2) in powder beds, where the inclusion experienced a higher magnitude of maximum shear stress at a relatively deeper depth inside the packing (at $\lambda_v = 3.5 d$, whereas in the case of the granular surrounding this occurs at $1.75 d$) (3) at some instances, a lower level of external load results in relatively higher stresses in the inclusions at some locations. This phenomenon occurs as a result of fluctuations within the system. Miller et al.²³ previously studied the effect of fluctuations in granular systems and report that fluctuations are emphasized in small size inclusions (as is the case here -1 cm), and (4) the distribution of the maximum shear stress within the sensor particle attains the maximum value inside the particle. This occurs around the center of the

inclusion in the case where it is surrounded by the powder bed. This suggests that, for this case, shear-induced yielding is most likely to occur at the center region of the inclusion rather than at the interparticle contact region (this mostly corresponds to granular surrounding). Further studies are required to characterize the yielding condition of the inclusions in relation to their surroundings.

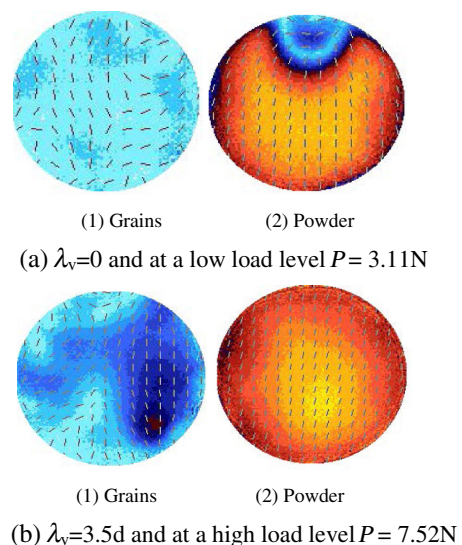


Fig. 8 Contours of maximum shear-stress distribution in the inclusion embedded in the particulate packing. The arrows show the direction of the major principal stress (color coded to the same scale as presented in Fig. 6).

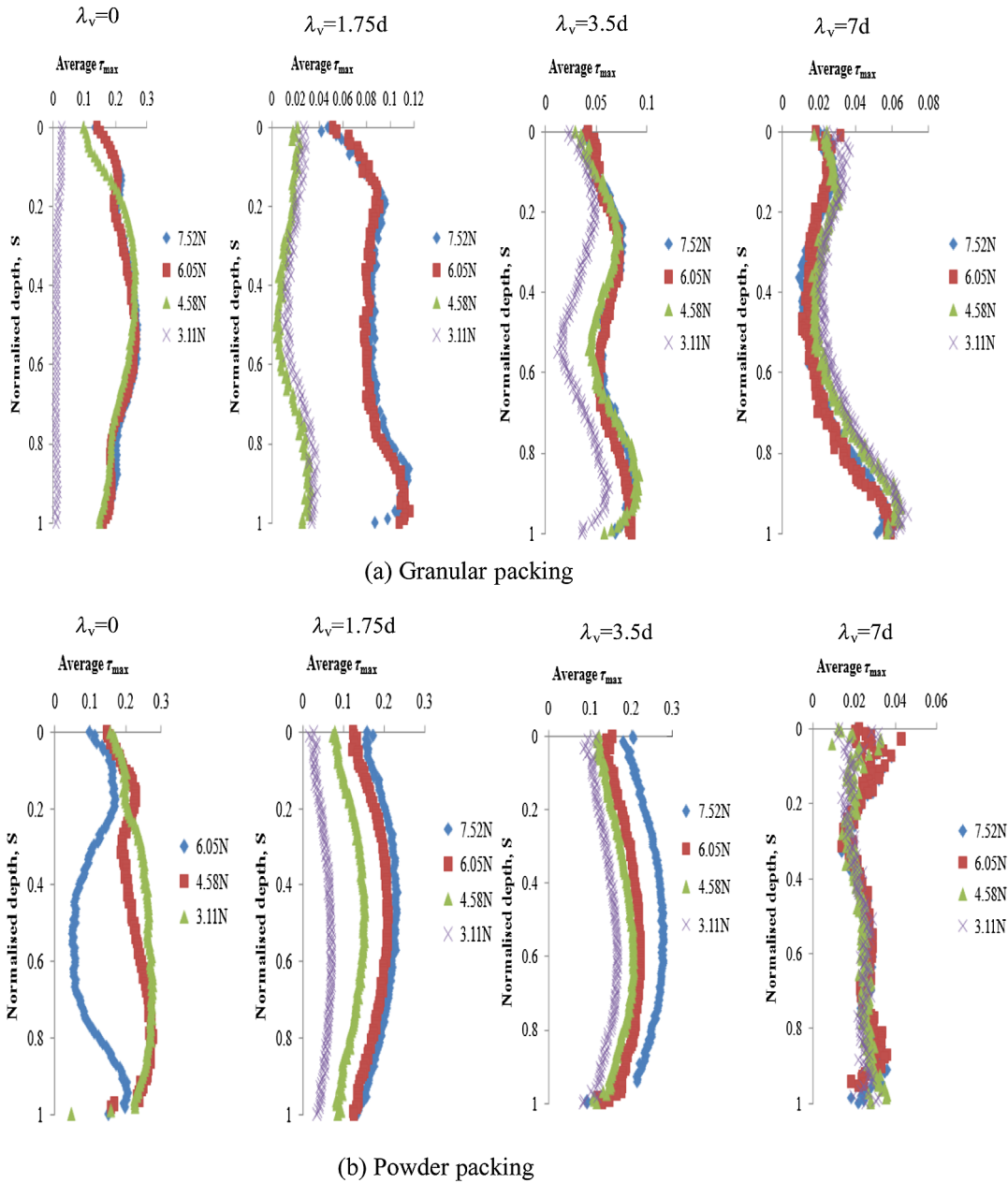


Fig. 9 Variation of average maximum shear stress (average τ_{max} in MPa) across the inclusion embedded at different elevations (λ_v) from the loading surface in particulate packing: (a) granular packing and (b) powder packing.

Figure 10 shows the estimate of the distance where maximum shear stress attains the peak value (z/a maximum) in the inclusions embedded in the granular packing compared with the predictions based on the Hertz theory.²¹ We point out that such an analysis for the case of inclusion in the powder bed is not presented here as perhaps it is not relevant. It is worth remembering that in the case of the inclusion embedded in the powder bed, the coordination number tends to be infinity, and the contact width “a” is disproportionately small when compared with the granular bed considered in this study. From Fig. 10 it can be observed that, in general, the experimental results of z/a differ significantly from predictions based on Hertz theory, especially when the inclusion is away from the loading surface ($\lambda_v > 0$). Although Hertz theory does not account for the

effects of interactions between the contiguous contacts, the analysis provides an indication of the strong effects of this that could result in multicontact particulate systems such as the inclusion considered in this study. This outcome has relevance to the DEM modeling of particulate systems as the methodology does not provide information on how stresses vary within the particle scale, an aspect desired in future studies for defining the strength criteria for individual particles under mechanical loading. Further analysis is required to understand why inclusions in some cases result in the position of the peak value in maximum shear stress slightly lower than that using Hertz analysis (e.g., $P \sim 6$ N). Also, the present study has used Hertz theory for obtaining the theoretical location of maximum shear stress occurring within the inclusions surrounded by the granular

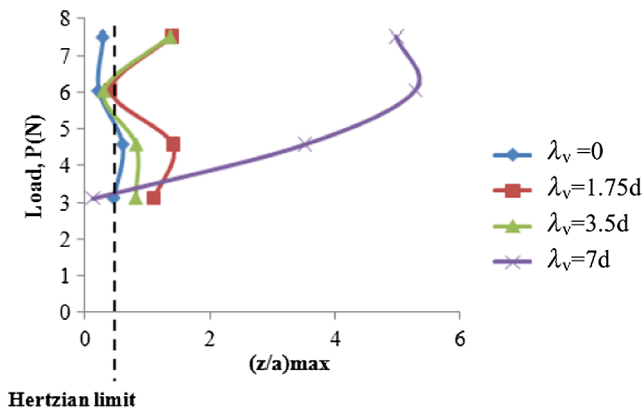


Fig. 10 Variation of maximum value of z/a for different locations (λ_v) of the inclusion embedded in granular packing.

system and this is compared with the current experimental results. This is reasonable considering that the grains have a very low value of angle of repose (Fig. 2). However, for relatively high frictional granular systems, models such as Hertz–Mindlin²² could be used for this purpose.

6 Conclusions

Stress transmission characteristics in particulate systems are exceedingly complex and are difficult to understand. However, the current research (quasithree-dimensional (3-D) using 3-D particles and a two-dimensional compression rig) has shown the effectiveness of applying photo stress analysis in understanding some of the stress transmission properties at a single-particle (inclusion) scale inside bulk particulate systems subjected to axial compression loading. Stress transmission within the inclusions occurs in a highly nonhomogeneous manner. Inclusions surrounded by powder materials display a strong and dominant deviatoric nature (as reflected by the values of maximum shear-stress distribution), whereas this nature diminishes in the case of granular surroundings. Generally, when the surrounding materials are made of powder, the system tends to act more like a continuum material and is shear dominant, as the direction of major principal stress displayed by the inclusion acts along the direction of axial loading. The relevance of the results to the existing assumption made in DEM modeling of particulate systems ignoring interaction effects of contacts is presented. It would be desirable to account for the variations of stresses within the single-particle scale by modeling the mechanical behavior of particulate systems as a multiscale problem. Further investigations could include the sensing state of the stress in the inclusions under different types of materials and wall boundaries. This would help to identify more realistic temporal and spatial conditions to prescribe the yielding of particulates as a function of size, material type, and positions held inside particulate packing under different loading environments. Comparison of the present results with other modeling methodologies such as FEM would also be desirable in the future.

Acknowledgments

This project was supported by the NSTIP strategic technologies program in the Kingdom Award No. 11-NAN1877-02.

References

1. L. Scholtes et al., "Micromechanics of granular materials with capillary effects," *Int. J. Eng. Sci.* **47**(1), 64–75 (2009).
2. T. G. Sitharam and M. S. Nimbkar, "Micromechanical modelling of granular materials: effect of particle size and gradation," *Geotech. Geol. Eng.* **18**(2), 91–117 (2000).
3. S. J. Antony, "Link between single-particle properties and microscopic properties in particulate assemblies: role of structures within structures," *Phil. Trans. R. Soc. A* **365**(1861), 2879–2891 (2007).
4. S. J. Antony and N. P. Krut'yan, "Role of interparticle friction and particle-scale elasticity in sheared-strength mechanism of three-dimensional granular media," *Phys. Rev. E* **79**(3 Pt 1), 031308 (2009).
5. S. J. Antony, "Evolution of force distribution in three-dimensional granular media," *Phys. Rev. E* **63**(1), 011302 (2000).
6. A. Drescher and J. de Jong, "Photoelastic verification of a mechanical model for the flow of a granular material," *J. Mech. Phys. Solids* **20**(5), 337–351 (1972).
7. T. S. Majmudar et al., "Jamming transition in granular systems," *Phys. Rev. Lett.* **98**(5), 058001 (2007).
8. D. M. Wood and D. Leśniewska, "Stresses in granular materials," *Granular Matter* **13**(4), 395–415 (2011).
9. P. A. Cundall and O. D. L. Strack, "A discrete numerical model for granular assemblies," *Geotechnique* **29**(1), 47–65 (1979).
10. S. J. Antony and R. M. Kuhn, "Influence of particle shape on granular contact signatures and shear strength: new insight from simulations," *Int. J. Solids Struct.* **41**(21), 5863–5870 (2004).
11. S. J. Antony and D. Chapman, "Probing shear stress distribution within single particle scale inside particulate packing," *KONA Powder Part. J.* **28**, 180–188 (2010).
12. X. Fu et al., "Application of X-ray microtomography and image processing to the investigation of a compacted granular system," *Part. Part. Syst. Charact.* **23**(3–4), 229–236 (2006).
13. C. Huan, X. Yang, and D. Candela, "NMR experiments on a three-dimensional vibrofluidized granular medium," *Phys. Rev. E* **69**(4 Pt 1), 041302 (2004).
14. J. Bridgwater, S. Forrest, and D. Parker, "PEPT for agglomeration?," *Powder Technol.* **140**(3), 187–193 (2004).
15. J. W. Dally and W. F. Riley, *Experimental Stress Analysis*, McGraw Hill, Singapore (1987).
16. E. A. Patterson, "Automated photoelastic analysis," *Strain* **24**(1), 15–20 (1988).
17. K. Ramesh, *Digital Photoelasticity*, Springer, New York (2000).
18. K. Ramesh and S. K. Mangal, "Data acquisition techniques in digital photoelasticity: a review," *Opt. Lasers Eng.* **30**(1), 53–75 (1998).
19. K. Ramesh, T. Kasimayan, and B. N. Simon, "Digital photoelasticity: a comprehensive review," *J. Strain Anal. Eng. Des.* **46**(4), 245–266 (2011).
20. H. Yang, S. Gibson, and R. A. Tomlinson, "Improvement of Fourier polarimetry for applications in tomographic photoelasticity," *Exp. Mech.* **46**(5), 619–626 (2006).
21. S. Albaraki, S. J. Antony, and C. Arowosola, "Visualising shear stress distribution inside flow geometries containing pharmaceutical powder excipients using photo stress analysis tomography and DEM simulations," *Proc. AIP* **1542**, 706–709 (2013).
22. K. L. Johnson, *Contact Mechanics*, Cambridge University Press, Cambridge (1985).
23. B. Miller, C. O'Hern, and R. P. Behringer, "Stress fluctuations for continuously sheared granular materials," *Phys. Rev. Lett.* **77**(15), 3110–3113 (1996).

Simon Joseph Antony is an associate professor at the Institute of Particle Science and Engineering, University of Leeds. He has more than 100 publications in reputed international journals and conference proceedings. He has won many awards, including the prestigious M.I.T Young Research Fellowship for Exemplary Research in Computational Mechanics and the Certificate of Merit as an Example of Outstanding Achievements in UK Particle Science and Technology by IChemE, UK. Presently, he serves as an editorial board member for several international journals and professional bodies.

Osas Imafidon received his MSc degree in chemical engineering at the University of Leeds. His interests include innovations in chemical, pharmaceutical, and process engineering. He is passionate about research and acquired analytical and experimental skills in powder processing.

Thabit Barakat is a professor in the Physics and Astronomy Department, King Saud University, Riyadh. He has made several publications in his area of expertise, including mathematical methods in quantum mechanics, perturbation theories, and quantum mechanical systems. His current research includes fundamental level studies on cohesive energies and thermal stabilities of metallic nanoparticles and their applications in particulate processes.